A comparative noise analysis and measurement for n-type and p-type pixels with CMS technique

Xiaoliang Ge[1], Bastien Mamdy[2,3], Albert Theuwissen[1,4]
[1]Delft University of Technology, Delft, Netherlands
[2]STMicroelectronics, Crolles, France
[3]Universite Claude Bernard Lyon 1, Villeurbanne, France
[4]Harvest Imaging, Bree, Belgium

Abstract

This paper presents a noise analysis and noise measurements of n-type and p-type pixels with correlated multiple sampling (CMS) technique. The output noise power spectral density (PSD) of both pixel types with different CMS noise reduction factors have been simulated and calculated in the spectral domain. For validation, two groups of test pixel have been fabricated with a state-of-the-art n-type and p-type CMOS image sensor (CIS) technology. The calculated and the measured noise results with CMS show a good agreement. Measurement results also show that the n-type and p-type pixels reach a 1.1 e^- and 0.88 h^+ input-referred temporal noise respectively with a board-level 64 times digital CMS and ×6 analog gain.

I. Introduction

The increasing requirement for better visualization under low light condition, especially in medical and diverse scientific field calls for the development of low-noise CMOS image sensors. Such image sensor will be capable of operating under photon-starved condition and capturing visually distinguishable images, while being more cost-effective, power-efficient [1] and providing higher spatial resolution than alternative imaging techniques [2]. Among different noise performance-improving techniques and structures, a p-type pixel has been considered as one of the promising candidate for low-noise CMOS image sensor. Thanks to the combination of a hole-based photo-detector coupled with dedicated pMOS transistors, p-type pixels could present several advantages over their n-type counterparts, including lower dark current, lower cross-talk and improved low frequency noise character [3]. However, compared with nMOS transistors, the use of pMOS as a source follower in p-type pixels suffers from a larger thermal noise due to its lower trans-conductance. Consequently, the doubled thermal noise power after correlated double sampling (CDS), together with the residual 1/f noise power, becomes one of the most significant factors that prevent p-type pixels temporal noise from achieving sub-carrier (electron or hole) level. As a circuit-level noise reduction technique, CMS has been proved very effective for thermal noise and 1/f noise reduction [4]. Hence, an analysis and measurement of the CMS noise reduction effect for p-type pixel in comparison with n-type ones is meaningful for further temporal noise minimization.

In this work, a temporal noise calculation and measurement, as well as a comparative analysis for n-type and p-type pixel targeted for low noise image sensor application is presented. At first, the noise PSD of in-pixel source followers in the frequency domain has been evaluated and different noise components have been analysed. Then, the CMS noise transfer characteristic for both n- and p-type pixels has been analysed in the frequency domain. Afterwards, the temporal readout RMS noise measurement for both pixels involving CMS has been performed. The measured results show that the input-referred temporal noise level of n-type and p-type pixels reach $1.1e^-$ and $0.88h^+$ respectively.

II. Noise analysis with CMS technique

A. Noise sources of pixel

For noise calculation, we regard the flicker noise and thermal noise originated from pixel part as the dominant source. Figure 1 shows the schematic of source followers used in n-type and p-type pixels as well as their noise equivalent circuit. The nMOS MN1 and pMOS MP1 are the pixel-level input transistor, MN2 and MP2 serve as the bias current source transistors which are implemented at the column-level.

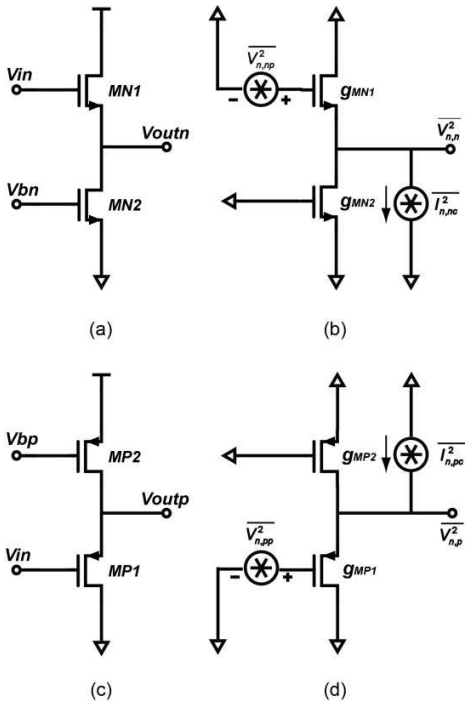

Figure 1 *Source follower schematic and equivalent circuit for noise analysis. (a) n-type source follower; (b) n-type source follower including noise sources; (c) p-type source follower; (d) p-type source follower including noise sources;*

An established fact for in-pixel source follower is that the driving source impedance is moderate while the input impedance is quite high. Therefore, the input-referred noise current source can

be neglected in the noise model, and only the noise voltage source is left [5]. Assuming all transistors operate in saturation, the noise PSD for n-type [6] and p-type source follower are then given by

$$S_{n,n}(f) = \overline{v_{n,n}^2} = \frac{8}{3}kT\frac{1}{g_{mn1}}\left(1+\frac{g_{mn2}}{g_{mn1}}\right) + \left[N_{fmn1} + \left(\frac{g_{mn2}}{g_{mn1}}\right)^2 N_{fmn2}\right]\frac{1}{f} \quad (1)$$

$$S_{p,n}(f) = \overline{v_{n,p}^2} = \frac{8}{3}kT\frac{1}{g_{mp1}}\left(1+\frac{g_{mp2}}{g_{mp1}}\right) + \left[N_{fmp1} + \left(\frac{g_{mp2}}{g_{mp1}}\right)^2 N_{fmp2}\right]\frac{1}{f} \quad (2)$$

where $k=1.3807\times10^{-23}J/K$ is the Boltzmann constant, T is the absolute temperature, f is frequency, g_{mn1}, g_{mn2}, $g_{mp1}$and g_{mp2} are trans-conductance; and N_{fmn1}, N_{fmn1}, N_{fmp1} and $N_{fmp1}$are flicker noise parameter of MN1, MN2, MP1 and MP2, respectively.

The noise power spectral densities of p-type and n-type pixels have been first extracted from the measurement. The measurement details will be mentioned in Section III. As shown in Figure 2, the p-type pixel exhibits less 1/f noise power density in low frequency region (10Hz ~50kHz) than the n-type one due to a naturally formed "buried channel" inside the pMOS transistor, which could carry the holes in the channel at some distance from the "dirty" oxide-silicon interface.

Moreover, the thermal noise or the noise floor is also obtained from the extracted data, which are 1.68×10^{-15} V^2/Hz for the p-type source follower and 2.76×10^{-15} V^2/Hz for the n-type one respectively. The thermal noise PSD in this feature is due to the fact that the thermal noise of source followers is determined by the trans-conductance g_{mn1} and g_{mp1}. If the input transistors in the n- and p-type pixels have the same width/length ratio and are biased with the same current, g_{mp1} for the pMOS transistor will be smaller than g_{mn1}as a result of a lower carrier mobility of holes.

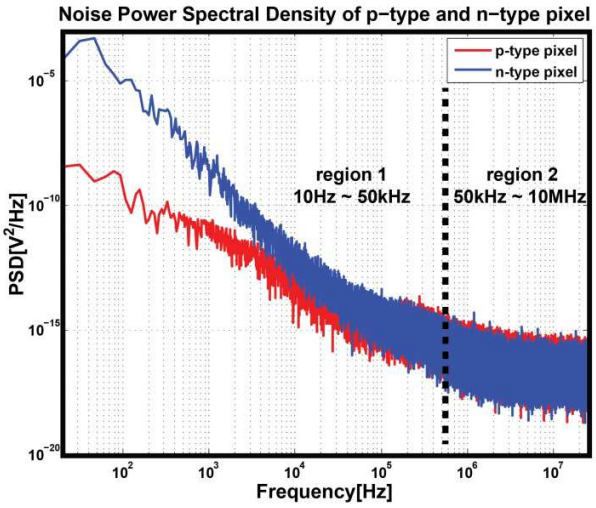

Figure 2 *The noise PSD for n-type and p-type pixel.*

B. CMS operation and noise reduction effect

The CMS operation has been considered as an alternative to the CDS operation for CIS system. The sampling diagram of CMS operation for CIS is depicted in Figure 3. In Figure 3, T_0 is the sampling period; $T_g=M_gT_0$ is the interval period between two groups of multiple sampling, where M_g is an integer. Firstly, reset levels ($V_{rst,1}$, $V_{rst,2}$... $V_{rst,M}$) and signal levels ($V_{sig,1}$, $V_{sig,2}$... $V_{sig,M}$) are sampled for M times sequentially. The delay between each correlated sampling levels (e.g. $V_{rst,1}$ and $V_{sig,1}$, $V_{rst,2}$ and $V_{sig,2}$) is $(M+M_g)T_0$. Then, the sum of reset levels and signal levels, which are obtained from M-times sampling, are subtracted from each other. Lastly, the final output can be achieved by dividing the differential result by the factor of M. In this way, on one hand, the correlated noise and the low frequency noise can be eliminated or reduced by the step of subtraction or differentiation, on the other hand, the input-referred thermal noise amplitude is reduced inversely proportional to $\sqrt{M}$thanks to the averaging effect [7].

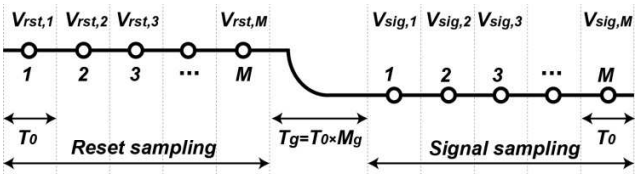

Figure 3 *The sampling diagram of CMS operation.*

Due to the differentiation and averaging procedures in the CMS configuration, the effectiveness of the CMS noise canceller can be characterized as a pass-band narrowing operation, as analysed in [8], or a noise power density reduction operation by oversampling.

First, consider that the noise reduction effect of CMS is the result of the bandwidth-narrowing operation. As interpreted by Figure 4, in the initial sampling phase, the signal is first sampled with the sampling circuits of a cut-off frequency f_c. Subsequently, the operation of subtracting two correlated levels acts as a discrete time high-pass filter with an equivalent cut-off frequency f_l, which is related to the time interval between two group sampling operations. Finally, the output noise power are low-pass filtered for the second time with another equivalent cut-off frequency $f_h>>f_c$ by virtue of the bandwidth limitation effect. Thus, the whole CMS operation can be equivalent to a continuous time band-pass filter of which the first zero f_l and first pole f_h are located at:

$$f_l = \frac{1}{2\pi(M+M_g)T_0} \quad (3)$$

$$f_h = \frac{\sqrt{2}}{\pi(M+M_g)T_0} \quad (4)$$

Therefore, the bandwidth of the band-pass filter can be defined as:

$$f_{BW} = \frac{2\sqrt{2}-1}{2\pi(M+M_g)T_0} \quad (5)$$

Figure 5 shows the equivalent transfer function of the CMS band-pass filter as a function of $(M+M_g)T_0$. With a fixed sampling period T_0, and an increasing M, the pass-band shifts to a higher

frequency region and its bandwidth becomes wider. As such more low frequency noise could be attenuated, while more thermal noise in the high frequency region will be integrated due to the wider bandwidth. On the other hand, if M is a constant value and T_0 increases, the resonant frequency and the bandwidth of the band-pass filter will also shift with the sampling period. Thus, the effectiveness of noise reduction for both 1/f noise and thermal noise is greatly depending on M or T_0.

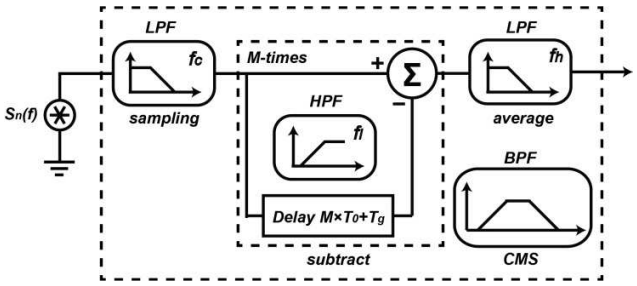

Figure 4 *The simplified model of a CMS circuit.*

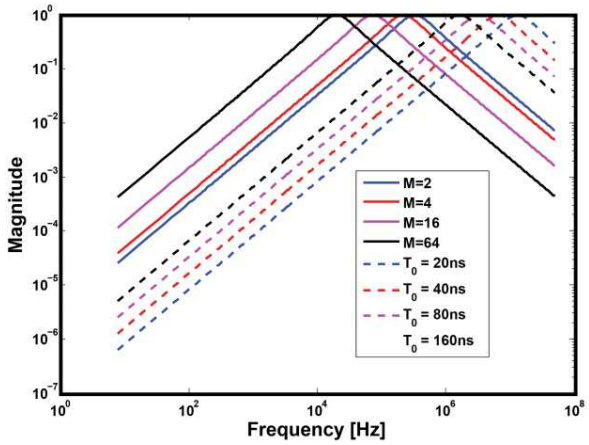

Figure 5 *Equivalent CMS band-pass transfer function*

Instead of considering the CMS thermal noise reduction effect as a bandwidth narrowing operation, it can be further characterized as an oversampling operation in terms of applying the sampling frequency higher than the Nyquist rate. If the sampling rate of CMS is increased from the Nyquist criterion $f_{s,ny}=1/(M+M_g)T_0$ to a new frequency $f_s=1/T_0$, the noise power density of the white band thermal noise is reduced with the ratio of the sample rates. Therefore, with a fixed sampling interval $(M+M_g)T_0$, as M increases, the thermal noise is reduced by a factor of $\sqrt{M}$ while the reduction of the 1/f noise in the low frequency region keeps the same for different M. Accordingly, for a given sampling interval, with a large value of M and a short sampling period T_0, a relatively small thermal noise can be obtained without sacrificing the reduction of the 1/f noise.

III. Noise calculation with CMS technique

On the basis of the above analysis, by employing the noise power spectrum density $S_n(f)$ from the pixel output and the system noise transfer function, the noise behaviour after CMS operation for n-type and p-type pixels can be modelled in MATLAB and their final integrated noise level can be estimated. The input noise PSD $S_n(f)$ used in this calculation are extracted from the test chip, which mentioned in Section II-A. What's more, the output noise power spectrum after CMS process can be expressed in frequency domain as:

$$\overline{v_{n,CMS}^2} = \frac{1}{M^2}\int_0^\infty S_n(f)\times\frac{1}{1+\left(\frac{f}{f_C}\right)^2}\times\left|H_{CMS}(f)\right|^2 df \tag{6}$$

where $H_{CMS}(f)$ equals to:

$$H_{CMS}(f) = \frac{2\sin(\pi f\cdot MT_0)\sin\left(\pi f\cdot(M+M_g-1)T_0\right)}{\sin(\pi f\cdot T_0)} \tag{7}$$

Figure 6 presents the calculated results. In Figure 6 (a) and (b), the noise PSD for both type pixels are calculated by using the constant sampling period T_0= 100ns and varied value for the number of sampling times M = 2, 4, 16 and 64. Note that as M increases, the noise PSD decreases at high frequency region and increases at low frequency region, which means that as a result of a longer interval period $(M+M_g)T_0$,with M increasing, the 1/f noise suppression effect by CMS operation is declined while thermal noise reduction tendency remains.

Figure 6 (c) and (d) shows the noise PSD as a function of sampling period T_0= 200ns, 400ns, 1600ns and 6400ns with a constant sampling number M =4. The noise PSD reduction for both 1/f noise and thermal noise are basically consistent with the result in (a) and (b), indicating that, except for M, an increased T_0 also leads to a lower resonant frequency for the pass-band bandwidth, thus reducing the effectiveness of CMS for 1/f noise reduction.

In Figure 6 (e) and (f), the noise PSD is obtained as a function of M = 2, 4, 16 and 64 within the fixed sampling interval $(M+M_g)T_0$ = 6.4µs. Obvious noise reduction in high frequency region can be observed while the noise PSD in low frequency region keeps almost the same with variant M. Thus, thanks to the oversampling operation, the white band thermal noise can be reduced effectively with an increased M while the effectiveness of low frequency noise reduction keeps the same.

In order to clarify and estimate the residue value of different noise components after CMS operation; the noise PSD in different frequency region (e.g. region 1 and 2, as shown in Figure 1) has been integrated separately. Figure 7 compares the n-type and p-type noise PSD after CMS operation as a function of M, where M = 1, 2, 4, 8, 16, 64 and T_0= 100 ns. As M = 1, the integrated noise in region 1 for the n-type noise is higher than that of the p-type noise, and lower in region 2, which indicates that a n-type pixel has a larger 1/f noise while a p-type pixel suffers from a higher thermal noise, which has been analysed in Section II-A. With M increasing, on one hand, the integrated noise level in high frequency region (region 2) for both type of pixels is suppressed until M = 64, with a factor of 72% for the n-type pixel and 80% for the p-type pixel respectively. On the other hand, the integrated noise amplitude in the low-frequency region (region 1) is gently increased in proportion to M. These results indicate that the low frequency noise, limit the total noise reduction effect of the pixel source follower.

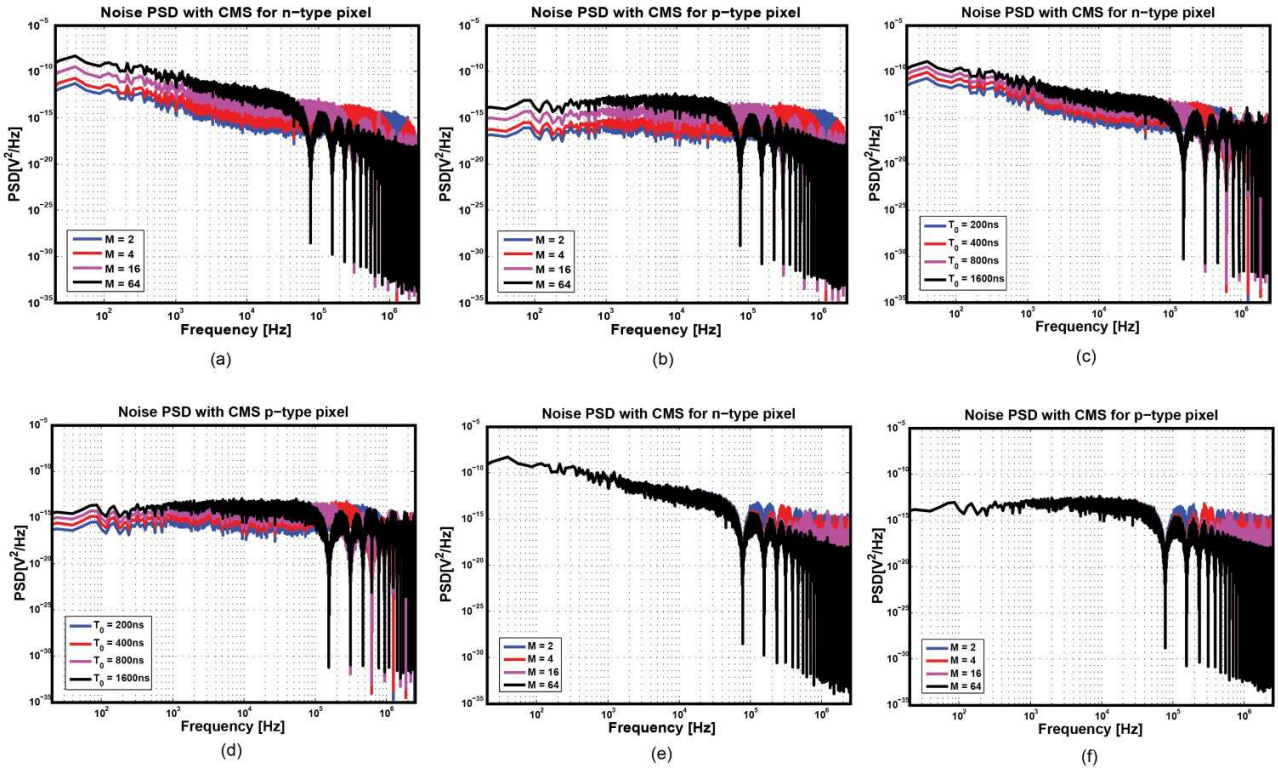

Figure 6 *Noise PSD for (a) n-type pixel with a sampling number M = 2, 4, 16, 64 and sampling period T_0 = 100ns; (b) p-type pixel with a sampling number M = 2, 4, 16, 64 and sampling period T_0 = 100ns; (c) n-type pixel with a sampling period T_0 = 200ns, 400ns, 800ns, 1600ns and sampling number M = 4; (d) p-type pixel with a sampling period T_0 = 200ns, 400ns, 800ns, 1600ns and sampling number M=4; (e) n-type pixel with a sampling number M = 2, 4, 16, 64 and $(M+M_g)T_0$ equals to a constant 6.4µs; (f) p-type pixel with a sampling number M = 2, 4, 16, 64 and $(M+M_g)T_0$ equals to a constant 6.4µs;*

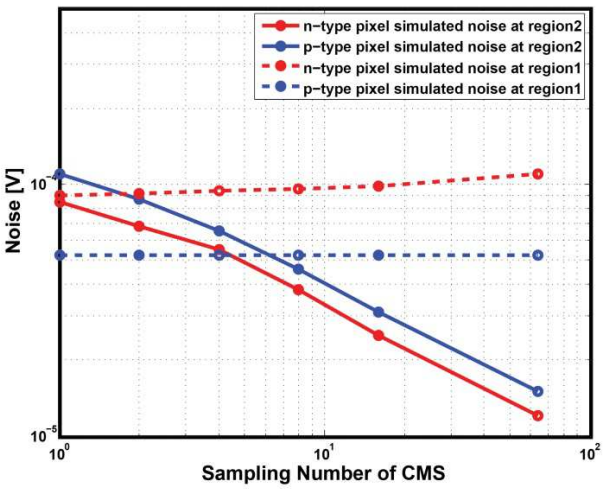

Figure 7 *Equivalent CMS band-pass transfer function*

In summary, based on the above calculation, the final noise reduction factor for the n-type pixel is 31% and for the p-type pixel noise is 50%.

IV. Noise measurement with CMS technique

In the measurements, the test pixels are divided into 2 sub-groups, one of which is fabricated with n-type pixel technology and the other one with p-type pixel technology. The front-end-of-line (FEOL) and back-end-of-line (BEOL) of both pixel types were designed and processed respectively in 90nm and 65nm technology. Both sub-groups feature the same pixel pitch of 2.5µm. As shown in Figure 8 (a) and (b), the 3D pixel structure isolated by deep trench isolation (DTI) technology integrates a back-side-illuminated buried vertically pinned-photodiode (BPD) as well as a planar transfer gate (TG) in each pixel [9][10]. Unlike the arrayed image sensor, the test chip includes only one effective pixel for each test structure owing to the area limitation. For both pixels, the gate width and length of the studied SF transistors are 0.2µm/0.7µm. The current sources for both SFs are set to 2µA.

In comparison with standard n-type pixels, all doping species type used to form the BPD and TG are inverted in the p-type pixel and the in-pixel MOS transistors are also switched from nMOS to pMOS. Hence, as can be seen from Figure 9, the transistor gate in the p-type pixel has to be driven low to switch on and high to switch off, while the timing remains the same.

Temporal noise characterization has been done in dark and implemented by using the reset voltage (VPIX) as an input for the SF and keeping TG and RST off during the measurement period. In order to reduce the impact of the PCB noise, an off-chip PGA with a gain of 6 has been implemented in the readout chain. The

RMS temporal noise is first measured by a board-level 16bit ADC and then referred to the carrier domain by dividing it with the measured conversion gain (CG). The sampling period T_0 = 100ns, which is the same as the calculated one, is used for both test chips. Instead of running a statistical analysis of spatial dispersion, the noise value given here is the histogram-based (fit to a Gaussian-like distribution) variance value of the output signal.

Figure 10 shows the measured plot of the noise variance as a function of the average output signal voltage value for both pixels. The conversion gain for the n-type and p-type pixel are 153μV/e^- and 110 μV/h^+ respectively.

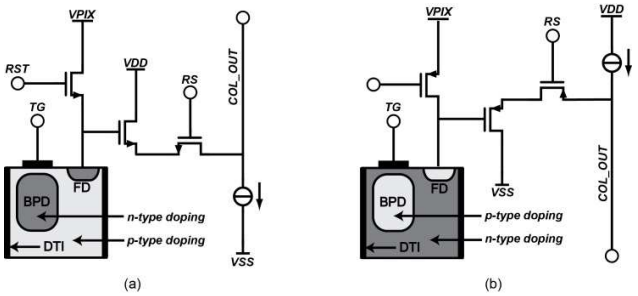

Figure 8 *Schematic with cross-section of BPD and TG region as well as readout architecture (a) n-type pixel; (b) p-type pixel.*

Figure 11 shows the measured input-referred noise for n-type and p-type pixels with a comparison to the simulation results both in the voltage and the carrier domain. In the calculation result described above, noise due to the sample and hold process is ignored. As a result of omission of aliasing effect in the calculation, there is a deviation between simulation and measurement value, which is around 20% for the n-type pixel and 22% for the p-type pixel. However, a good agreement between the measured and calculated results shows an identical noise reduction factor by CMS for both types of pixels, demonstrating the validity of the noise calculation by using the noise transfer function.

As predicted by the noise calculation, the measurement result shows noise reduction tendency as the sampling number of CMS increases. Moreover, it also indicates that the low-frequency random noise of the pixel source follower limits the noise reduction effect as the number of sampling times increases. As shown in Figure 11 (a), compared to the p-type pixel, the n-type pixel shows a limited noise improvement from 8-times CMS. However, the p-type pixel prevents this limitation up to 64-times thanks to a lower 1/f noise coefficient. Comparing the input-referred noise with only-digital CDS, the CMS noise reduction factor is around 24% for n-type pixels and 45% for p-type pixels when 64-times CMS is applied. For M = 1, 2, 4 and 8, the noise level in charge domain for an n-type pixel is lower than a p-type pixel thanks to a larger CG. However, for M = 16 and 64, the residual 1/f noise in nMOS SF limits the further noise reduction and the noise level of the p-type pixel becomes lower than that of the n-type one. As indicated in Fig.5 (b), for M = 64, the n-type pixel features an input-referred noise of 1.1e^- and the p-type pixel shows a lower noise level at 0.88 h^+.

Consequently, both simulated and measured results show that the incorporation of CMS operation and a p-type pixel can present a better noise reduction effect as compared to the n-type one.

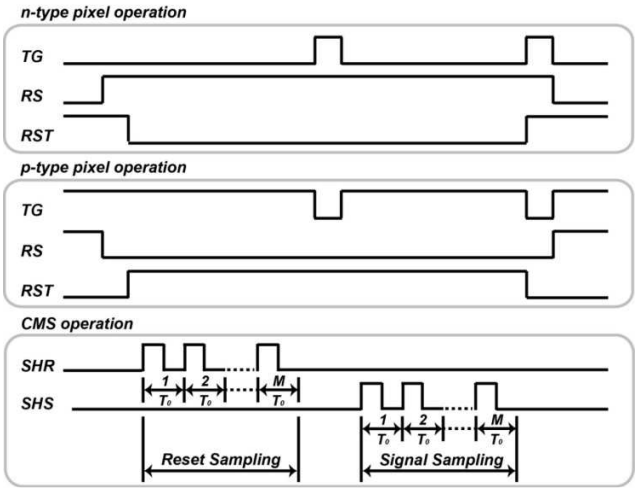

Figure 9 *Timing diagram of the readout sequence for n-type pixel, p-type pixel and CMS operation.*

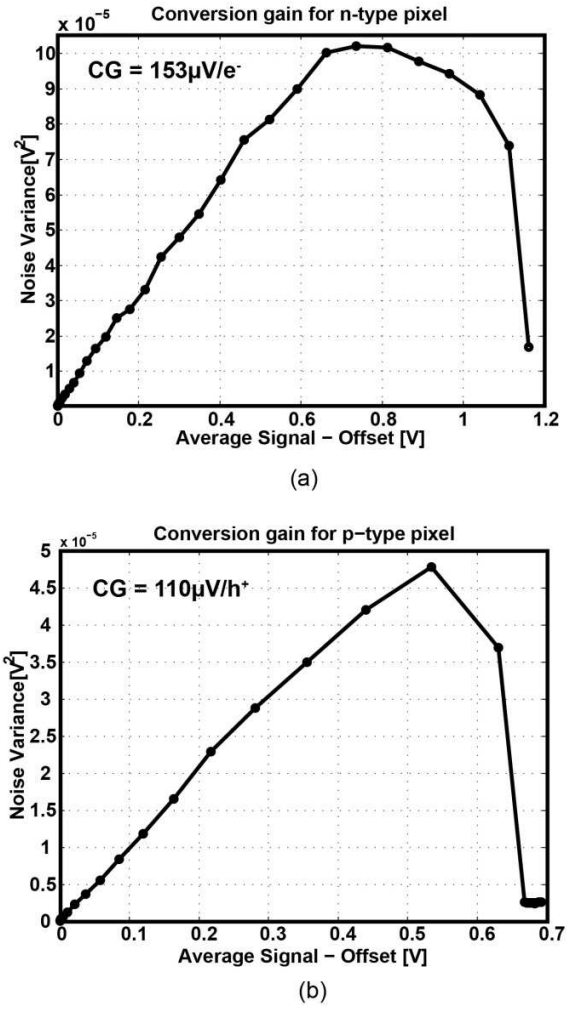

Figure 10 *Conversion gain for (a) n-type pixel; (b) p-type pixel*

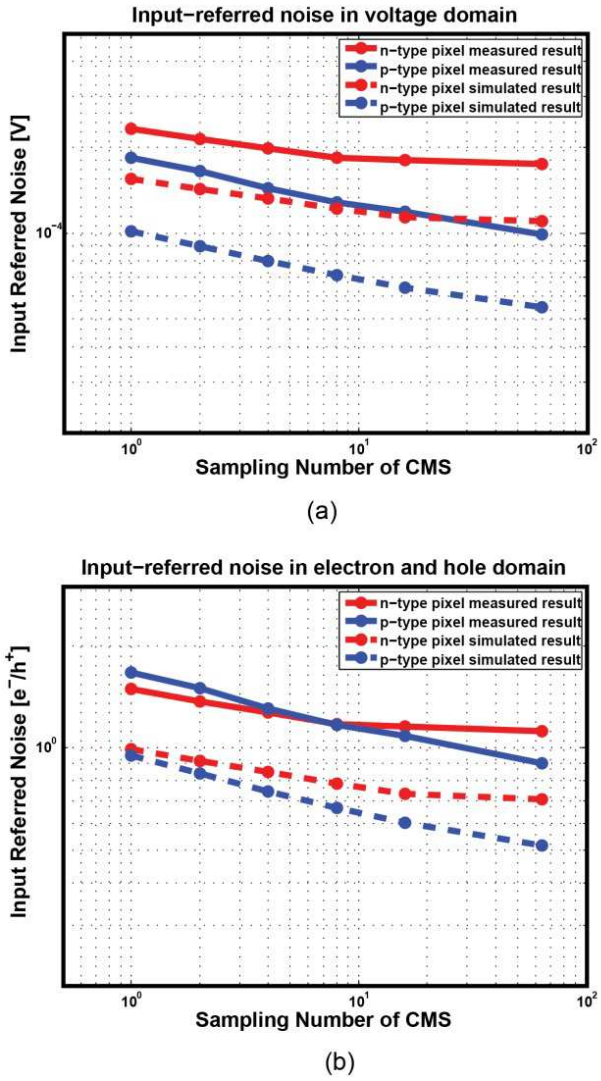

Figure 11 *Input-referred noise for measured and simulated results (a) in voltage domain; (b) in electron and hold domain.*

IIV. Conclusion

In this paper, we first explore the noise reduction effect of CMS on the noise PSD of n-type and p-type pixels. Based on the noise PSD and transfer function of CMS, the residual noise of both types of pixels has been calculated. Subsequently, we measured the temporal noise of n- and p-type pixels with CMS technique. A good agreement between calculated and measurement results shows that the noise performance improvement brought by CMS has been demonstrated theoretically and experimentally. With a board-level ×6 analog gain, the n-type and p-type pixel achieve a temporal noise level of $1.1e^-$ and $0.88h^+$respectively after 64 times digital CMS during the readout phase.

Acknowledgment

The authors would like to thank Francois Roy, STMicroelectronics, for his dedicated support and invaluable help.

Reference

[1] P.Seitz and A.J.P.Theuwissen, Eds., Single-Photon Imaging, Berlin, Germany: Springer, 2011, ISBN 978-3-642-18443-7, pp. 38-39.

[2] E.R.Fossum, “Modelling the Performance of Single-Bit and Multi-Bit Quanta Image Sensors,” IEEE Journal of The Electron Devices Society, Vol. 1, No. 9, pp. 166-174, Sep. 2013.

[3] E.Stevens, et al., “Low-Crosstalk and Low-Dark-Current CMOS image sensor technology using a Hole-Based Detector,” in IEEE ISSCC, 2008, pp. 60-595.

[4] S.Kawahito, et al., ”Noise reduction effects of column-parallel correlated multiple sampling and source-follower driving current switching for CMOS image sensors”, in IISW, Bergen, Norway, 2009.

[5] B. Razavi, Design of Analog CMOS Integrated Circuits: McGraw-Hill, 2001, ISBN 0-07-118815-0, pp. 231-232.

[6] N. Kawai, et al., “Noise analysis of high-gain low-noise column readout circuits for CMS image sensor”, IEEE Trans. Electron Dev., vol.51, no.2, pp.185-194, 2004.

[7] S. Kawahito, et al., “Column parallel signal processing techniques for reducing thermal and random telegraph noises in CMOS image sensors”, in IISW, Ogunquit, USA, 2007

[8] S.Suh, et al., “Column-parallel correlated multiple sampling circuits for CMOS image sensors and their noise reduction effects”, in Sensors 2010, vol.10, pp. 9139-9154, 2010.

[9] J.Michelot, et al., “Back Illuminated Vertically Pinned Photodiode with in Depth Charge Storage”, in IISW, Hokkaido, Japan, 2011.

[10] B. Mamdy, et al., “A low-noise, P-type, vertically-pinned and back-side-illuminated pixel structure for image sensor applications”, in IISW, Vaals, the Netherlands, 2015.